

1 **Changes in the [Intermediate](#) Water Mass**
2 **Formation Rates in the Global Ocean for the**
3 **Last Glacial Maximum, Mid-Holocene and**
4 **Pre-Industrial Climates**

I. Wainer

5 Universidade de São Paulo, São Paulo, Brazil

M. Goes

6 University of Miami/CIMAS and NOAA/AOML, Miami, Florida

L. N. Murphy

7 Lawrence Berkeley National Laboratory, Berkeley, California;

8 now at: University of Miami/RSMAS, Miami, Florida

E. Brady

9 National Center for Atmospheric Research, Boulder, Colorado

Corresponding Author: I. Wainer (wainer@usp.br); Universidade de São Paulo, São Paulo,
Brazil

10 The paleoclimate version of the National Center for Atmospheric Research
11 Community Climate System Model **version 3** (NCAR-CCSM3) is used to an-
12alyze changes in the water formation rates in the Atlantic, Pacific, and In-
13dian Oceans for the Last Glacial Maximum (LGM), Mid-Holocene (MH) and
14 Pre-Industrial (PI) control climate. During the MH, CCSM3 exhibits a north-
15 south asymmetric **response** of intermediate water subduction changes in the
16 Atlantic Ocean, with a reduction of 2 Sv in the North Atlantic, and an in-
17crease of 2 Sv in the South Atlantic relative to PI. During the LGM, there
18 is increased formation of intermediate water, and a more stagnant deep ocean
19 in the North Pacific. The production of North Atlantic Deep Water (NADW)
20 is significantly weakened. The NADW is replaced in large extent by enhanced
21 Antarctic Intermediate Water (AAIW), Glacial North Atlantic Intermedi-
22ate Water (GNAIW) and also by an intensified of Antarctic Bottom Water
23 (AABW), with the latter being a response to the enhanced salinity and ice
24 formation around Antarctica. Most of the LGM intermediate/mode water
25 is formed at $27.4 < \sigma_{\theta} < 29.0 \text{ kg/m}^3$ while for the MH and PI most of the sub-
26duction transport occurs at $26.5 < \sigma_{\theta} < 27.4 \text{ kg/m}^3$. The simulated LGM South-
27ern Hemisphere winds are more intense by 0.2-0.4 dyne/cm^2 . Consequently,
28 increased Ekman transport drives the production of intermediate water (low
29 salinity) at a larger rate and at higher densities when compared to the other
30 climatic periods.

1. Introduction

31 Ventilation in the Southern and in the Arctic oceans contribute to significant uptake
32 of heat and atmospheric gases. In this respect, the intermediate waters are recognized
33 to have a major impact on the oceanic sink for anthropogenic CO₂ [e.g., *Sabine et al.*,
34 2004; *Sabine and Tanhua*, 2010], but also to contain the largest uncertainties in carbon
35 inventories [e.g., *McNeil et al.*, 2003]. The role of the formation of intermediate waters, in
36 particular the Antarctic Intermediate Water (AAIW), and their ability to redistribute heat
37 and freshwater within the upper ocean has been the subject of many studies [*Pahnke and*
38 *Zahn*, 2005; *Sloyan and Rintoul*, 2001; *Sørensen et al.*, 2001; *Sloyan and Kamenkovich*,
39 2007].

40 The AAIW is a low salinity water mass that is formed in the South Atlantic and
41 South Pacific oceans [*Taft*, 1963], and transported northward into the Indian, Pacific and
42 Atlantic along subtropical gyres. AAIW fills most of the Southern Hemisphere, and parts
43 of the North Pacific and North Atlantic Oceans at about 800 to 1200 m depth or within
44 $\sigma_{\theta} = 26.9 - 27.5 \text{ kg/m}^3$ isopycnals [*Talley*, 1996]. AAIW has been defined as the densest
45 class of the Subantarctic Mode Water (SAMW) [*McCartney*, 1977], with which it shares
46 similar dynamics [*Drijfhout et al.*, 2005]. In the formation region, AAIW (and SAMW)
47 is characterized by a thick (low potential vorticity) outcropping mixed layer just north
48 of the Subantarctic Front (SAF), with formation associated with the winter properties of
49 the mixed layer and winds [*Karstensen and Quadfasel*, 2002].

50 In the South Pacific, the intermediate waters that spread northward from the Southern
51 ocean are also denominated the Pacific Intermediate Water (PIW) [*Talley*, 1999]. The

52 North Pacific is currently the only place in the Northern Hemisphere that forms waters
53 at intermediate depths, the North Pacific Intermediate Water (NPIW), which is formed
54 between $\sigma_\theta = 26.2 - 26.9 \text{ kg/m}^3$ and is found generally north of 15°N , at depths of 300
55 to 800 m [*Talley, 1993*].

56 Underneath the intermediate waters are the deep waters. The North Atlantic Deep
57 Water (NADW) formation occurs at a high rate in the North Atlantic through convection
58 in the Arctic ocean, which makes the Atlantic high ventilated in these depths. In the
59 North Pacific the present abyssal circulation flows from the south, upwells to mid-depth
60 and returns south as the Pacific Deep Water (PDW) below the NPIW [*Schmitz, 1996*].
61 Below 4000 m, the cold and fresh Antarctic Bottom Water (AABW) occupies the ocean
62 across the globe.

63 Previous modeling and observational paleoclimate studies [*Adkins et al., 2002; Pahnke*
64 *et al., 2008, , and references therein*] have shown that the structure of the water masses
65 we know today has experienced considerable changes. For instance, proxy reconstructions
66 of the Last Glacial Maximum (LGM) [*Adkins et al., 2002*] show that the deep oceans
67 were more homogeneous, with stronger influence from the southern waters, which were
68 much saltier than they are today. The North Atlantic was much fresher, and the NADW
69 formation was suppressed, giving rise to a fresh north Atlantic intermediate formation
70 (GNAIW). In the North Pacific, proxy data ($\Delta^{14}\text{C}$) suggest a more vigorous and expanded
71 NPIW within the 1500-2000 m water column during the LGM, with a smaller exchange
72 from deep to intermediate waters [*Toggweiler, 1999; Matsumoto et al., 2002*]. This process
73 would be responsible for increasing deep carbon reservoirs in the deep Pacific Ocean during

74 the LGM [*Herguera et al.*, 2010]. The storing and release of heat, carbon and other ocean
75 tracers can contribute significantly, and potentially trigger changes in the earth's climate
76 system [*Cleroux et al.*, 2011; *Skinner et al.*, 2010]. Changes in water properties are in part
77 a consequence of subduction, and wind and mixing driven processes, as well as changes
78 in the ocean interior that occur after subduction [*Wong et al.*, 1999; *Joyce et al.*, 1998].

79 **In this study, we quantify the rate of water formation across the base of the mixed layer**
80 **for past climates.** We analyze simulation results for the LGM (approximately 21,000 years
81 before present), the Mid-Holocene (MH, approximately 6,000 years before present) and the
82 Pre-Industrial control (PI). These simulations are performed with the National Center for
83 Atmospheric Research (NCAR) Community Climate System Model version 3 (CCSM3),
84 which are described in detail in *Otto-Bliesner et al.* [2006]. Our main motivation is to
85 understand the response of the global subduction rates to the integrated changes during
86 past climates, such as the hydrological cycle, ocean temperature conditions, greenhouse
87 gases concentrations and orbital forcing, and their link to the related changes in the water
88 mass properties. Previous modeling studies analyzed these paleo climates in terms of
89 3-dimensional circulation [*Clauzet et al.*, 2007; *Otto-Bliesner et al.*, 2007], NADW and
90 AABW water mass formation [e.g., *Shin et al.*, 2003b; *Liu et al.*, 2005], and tropical
91 variability [e.g., *Liu et al.*, 2000; *Braconnot et al.*, 2007b; *Otto-Bliesner et al.*, 2009].
92 We improve the current knowledge by focusing on the AAIW formation and changes in
93 intermediate depths, and determine plausible mechanisms for such changes. This paper
94 is organized as follows: Section 2 describes the model and model experiments. Section 3

95 describes the general water mass features in the model simulations and their subduction
96 properties. Section 4 includes discussions of the results and conclusions.

2. Model Description

97 The CCSM3 is a coupled climate general circulation model consisting of four main
98 components, the atmosphere, ocean, sea ice and land. The atmospheric model is the
99 NCAR Community Atmosphere Model version 3 (CAM3), a three-dimensional primitive
100 equation model solved with the spectral method in the horizontal [*Collins et al.*, 2006].
101 The ocean model is the NCAR implementation of the Parallel Ocean Program (POP), a
102 three-dimensional primitive equation model in spherical polar coordinates with a dipole
103 grid and a 40 level vertical z coordinate [*Gent et al.*, 2006]. Poles are located in Greenland
104 and Antarctica.

105 The sea ice model is a dynamic–thermodynamic model, which includes a subgrid-scale
106 ice thickness parameterization and elastic–viscous–plastic rheology [*Briegleb et al.*, 2004].
107 It includes sea ice dynamics and exchanges of salt between sea ice and the surrounding
108 ocean. The land model includes a river routing scheme and specified land cover and plant
109 functional types [*Dickinson et al.*, 2006]. The atmosphere and land components share a
110 horizontal resolution of T42, approximately 2.8° in latitude and longitude. The ocean and
111 sea ice components share a horizontal resolution that is approximately 1° in latitude and
112 longitude with higher resolution in the Tropics and North Atlantic.

113 Concentrations of the atmospheric greenhouse gases in the **CCSM3** paleo simulations are
114 adjusted based on ice core measurements [*Flückiger et al.*, 1999; *Daellenbach et al.*, 2000;
115 *Monnin et al.*, 2001] and follow the protocols established by PMIP2 [*Braconnot et al.*,

116 2007a]. Their overall effect are a reduction in radiative forcing of -2.76 W m^{-2} for the
117 LGM and only -0.07 W m^{-2} for the mid-Holocene, with the latter only due to a reduction
118 in methane concentration. In addition to reduced atmospheric greenhouse gases, other
119 major differences are the changes in the earth's orbital parameters, the presence of ice
120 sheets, and exposed coastline and shallow sills due to sea level lowering. In the LGM,
121 elevation and ice sheet extent are taken from the ICE-5G reconstruction [*Peltier*, 2004].
122 Major changes include increased elevation and ice extent over Antarctica, the Southern
123 Andes and throughout much of the high latitude Northern Hemisphere, with the exception
124 of central Greenland. MH uses the same topography and ice elevation data as PI. The
125 solar constant is set to 1365 W m^{-2} in all three simulations. The model components are
126 integrated separately to obtain an appropriate initial state of the coupled system prior
127 to full coupling. The numerical simulations of the MH and LGM (except for the ocean)
128 are initialized from the PI run. The LGM ocean is initialized with a previous LGM
129 simulation *Shin et al.* [2003a]. Both are run for 300 years. At this time, as discussed
130 in *Otto-Bliesner et al.* [2006], the simulations reach quasi-equilibrium, with small trends
131 present, particularly at Southern Hemisphere high latitudes and the deep ocean. The
132 mean climate results analyzed are averages for the last 150 years of the LGM and MH
133 runs. A detailed description of the paleoclimate model and experiments are discussed in
134 *Otto-Bliesner et al.* [2006] and *Clauzet et al.* [2007].

3. Results

3.1. General features

135 Changes in the annual surface ocean response during the LGM and MH glacial periods
136 in comparison to the present day have been extensively discussed in previous modeling
137 studies [e.g., *Liu et al.*, 2000, 2003; *Shin et al.*, 2003a, b; *Otto-Bliesner et al.*, 2006, 2007;
138 *Clauzet et al.*, 2007, 2008; *Otto-Bliesner et al.*, 2009]. Here, for the sake of completeness,
139 we summarize the general hydrography and atmospheric fluxes in CCSM3.

140 The spatial changes in the intensity of the time-averaged zonal wind stress is shown in
141 Figure 1. In the Southern Hemisphere, there is a strengthening of the westerlies (positive
142 anomalies) in the LGM. Because of the complex topography, LGM winds are more intense
143 on the Pacific side of the South American coast and weaker on the Atlantic side. Between
144 40°S and the equator, wind changes are **smaller**. In the Northern Hemisphere there is a
145 shift of the zero wind stress curl southward in the LGM, but no visible shift is seen in the
146 Southern Hemisphere, **consistent with *Shin et al.* [2003a]**.

147 The mean zonal wind anomalies for the MH (not shown) are an order of magnitude
148 smaller than the ones in the LGM. Previous studies [e.g., *Liu et al.*, 2003] show substantial
149 changes of the seasonal wind stress during the MH, but small changes in the annual mean
150 because seasonal wind anomalies tend to be opposite in winter and summer in response
151 to the anomalous insolation forcing.

152 The CCSM3 LGM **global annual sea surface temperature (SST)** is on average 4.5°C
153 cooler relative to PI conditions [*Otto-Bliesner et al.*, 2006], which is stronger than ocean
154 cooling of 2°C in previous LGM simulations [*Shin et al.*, 2003a, b] and SST proxy recon-
155 struction (CLIMAP, 1981). The ocean surface is colder and saltier in most of the places

156 (Figure 2), caused by a weaker hydrological cycle due to a colder climate. High sea surface
157 salinity (SSS) anomalies of ≈ 7 psu are observed in the North Atlantic, and the highest
158 temperature anomalies are found in the North Pacific and North Atlantic, which is related
159 not only with brine rejection due to more ice formation, but with the migration of the
160 subtropical gyres southward (Figure 2). Warming in the Bering Sea and Gulf of Alaska
161 are related to changes in the upper level dynamics and a deepened Aleutian low, which
162 advects warm air poleward into the Gulf of Alaska *Otto-Bliesner et al.* [2006].

163 A comparison of the LGM simulation used here with proxy data from the South Atlantic
164 Ocean has been previously performed by *Clauzet et al.* [2008], which shows some regional
165 discrepancies. The largest biases occur in the eastern, equatorial and in the high latitudes
166 of the basin, while a good agreement between the model and reconstructed data is reached
167 in the western and central parts of the South Atlantic.

168 The annual mean surface temperature and salinity anomalies in the MH relative to PI
169 are less substantial than in the LGM (Figure 2b,d). Overall, there is a symmetric response
170 that reveals a tropical cooling and high latitude warming. This feature agrees with the
171 differences shown in Figure 2 and is consistent with a synthesis of mid-Holocene paleo-
172 SST records [*Liu et al.*, 2003]. Previous studies [*Otto-Bliesner et al.*, 2006] show that
173 Increased boreal summer insolation reduces Northern Hemisphere sea-ice, which enhances
174 the warming due to the ice-albedo feedback. Melting of sea-ice leads to a freshening of the
175 northern high latitudes, as observed in Figure 2b. High positive salinity anomalies located
176 in the North Pacific (≈ 0.8 psu) and Tropical Atlantic (≈ 0.2 psu) are due to atmospheric
177 drying *Braconnot et al.* [2007a].

178 These surface differences from the paleo simulations against the PI reflect changes in
179 the whole water column. Regarding the PI, zonally averaged sections of temperature
180 and salinity with depth (Figures 3 and 4, upper panels) show that the North Atlantic is
181 characterized by strong formation of relatively cold (about 2 to 4 °C; Figure 3a) and salty
182 (about 35 psu; Figure 4a) NADW at about 3000 m. In the South Atlantic, the low salinity
183 AAIW tongue is observed at about 1000 m, mostly south of the equator (Figure 3a). The
184 formation region of the AAIW (at about 50 °S) is characterized by a salinity minimum
185 between the $\sigma_\theta = 26.5\text{--}27 \text{ kg/m}^3$ isopycnals. In the Indo-Pacific, deep waters (below 1500
186 m) are generally colder ($\approx 0\text{--}2 \text{ °C}$; Figure 3b) and fresher ($\approx 34.6 \text{ psu}$; Figure 4b) than the
187 Atlantic counterpart, and low salinity intermediate waters (PIW and NPIW) fill most of
188 the basin between 1000–2000 m (Figure 4b). An excess of precipitation over evaporation
189 results in lower salinity values over the North Pacific. As a result the North Pacific shows
190 a stronger stratification and shallower mixed layer, favoring formation of lower density
191 waters with respect to the North Atlantic.

192 Significant differences are manifested in the hydrographic fields of the LGM (Figures
193 3c, d and 4c, d). In the North Atlantic, the deep signature of the NADW is not observed
194 during the LGM (Figure 4c). Instead, stronger formation of southern bottom waters ad-
195 vect strong salinity anomalies $> 1.5 \text{ psu}$ below 1500 m (Figure 3c), confining the northern
196 water formation to the upper 1500–2000 m of the water column. North Atlantic water
197 formation is more than 4°C colder than the PI, but relatively fresher in comparison to
198 the AABW in the LGM, therefore forming a tongue of Glacial North Atlantic Interme-
199 diate Water (GNAIW). In the Southern Ocean, the LGM features a much denser and

200 wider Antarctic Bottom Water (AABW) (Figure 4c, d), in agreement with proxy obser-
201 vations [Adkins *et al.*, 2002; Marchitto and Broecker, 2006], indicating a stronger AABW
202 formation. The Southern Ocean, which is the source region for the AABW, contains
203 higher surface salinity and lower temperature (Figure 4a, b) in the LGM. These surface
204 characteristics have been associated with an enhanced, colder and saltier AABW due to
205 intensified ice formation around Antarctica [Shin *et al.*, 2003a; Liu, 2006].

206 In the South Indo-Pacific, as observed in the South Atlantic during the LGM, formation
207 of AABW and Pacific Deep Water (PDW) are increased (Figure 4d). The volume increase
208 of the PDW displaces the LGM intermediate waters in the Indo-Pacific to shallower depths
209 (above 800 m). The intermediate waters suffer the highest temperature anomalies in the
210 Indo-Pacific, up to -3.5°C .

211 The density contours in Figures 3c, d and 4c, d suggest a higher stratification in the
212 upper 1500 m during the LGM, and a more homogeneously cold and stagnant deep layer
213 in the Pacific (4d). For instance, the $\sigma_{\theta} = 29 \text{ kg/m}^3$ density level is around 1000-1500
214 m depth in the LGM (Figures 4c, d), at about the same depth of the $\sigma_{\theta} = 27.5 \text{ kg/m}^3$
215 density level in the PI and MH (Figures 4a, b, e, f).

216 The hydrographic differences of the MH relative to PI are mostly restricted to the upper
217 1500 m (Figure 3e, f). Changes in the MH are largely due to anomalous seasonal insolation
218 [Liu *et al.*, 2003]. In agreement with [Liu *et al.*, 2003], the Pacific ocean changes in the MH
219 are characterized by a cooling and freshening in the Northern Hemisphere and a warming
220 in the Southern Hemisphere (Figure 3f). However, the Atlantic ocean shows warming in
221 the high northern latitudes, related to sea-ice reduction and resulting ice-albedo feedback.

222 As oppose to the upper layers, below 1500 m the MH is in general slightly saltier (order
223 of 10^{-3} psu) and warmer (order of 10^{-2} °C).

224 The density range of each water mass can be retrieved with a good approximation by
225 their θ -S properties. Here we use θ -S diagrams to select the σ_θ ranges of the main wa-
226 ter masses for the different geological periods in the Pacific, Indian, and Atlantic basins
227 (Figure 5). The potential temperature and salinity fields are first interpolated onto po-
228 tential density surfaces, similarly to *Downes et al.* [2010], and then averaged over each
229 basin between 15 – 60 degrees of latitude. [Previous model studies have already shown \$\theta\$ -S](#)
230 [relationships for the LGM and MH \[e.g., *Shin et al.*, 2003a; *Liu et al.*, 2005; *Otto-Bliesner*](#)
231 [et al., 2006\], and their comparison to the \$\theta\$ -S obtained from proxy data \[*Adkins et al.*,](#)
232 [2002\] suggests reasonable agreement with observations.](#)

233 During the PI an MH, the salinity minimum of approximately 34.2 representing the
234 AAIW core is observed at about $\sigma_\theta = 27.2$ kg/m³ in the South Atlantic and South Pacific
235 (5c,d). Considering the SAMW and AAIW together, their range spans from $\sigma_\theta = 26.4$ –
236 27.4 kg/m³. In the South Atlantic (Figure 5c), the MH shows a clear upward displacement
237 in the mean θ -S, and therefore a small warming (on the order of 0.03 °C) in the deep layers
238 relative to the isopycnals.

239 In the LGM the AAIW salinity minimum is denser, centered at about $\sigma_\theta = 28.0$ kg/m³
240 (Figure 5c, d), and with broader AAIW + SAMW range of $\sigma_\theta = 27.4$ – 29.0 kg/m³. Below
241 $\sigma_\theta = 28.0$ there is an almost linear increase in salinity and accompanying decrease in
242 temperature all the way to the bottom in the Pacific and South Atlantic. This behavior
243 is consistent with the extension of the PDW in the Pacific and AABW in the Pacific and

244 Atlantic, which is a feature attributed to the ocean during the LGM [e.g., *Clauzet et al.*,
245 2007; *Fischer et al.*, 2010; *Oppo and Fairbanks*, 1987].

246 In the North Pacific (Figure 5b), the NPIW minimum in the MH (34.5) is larger than
247 in the PI (34.3), but in both periods the minimum is located at about $\sigma_\theta = 26.4 \text{ kg/m}^3$,
248 with total range of 25.7–26.8 kg/m^3 . Between PI and MH the differences in deeper waters
249 are negligible. In the LGM, the glacial NPIW minimum of 34.8 is centered at $\sigma_\theta = 27.0$
250 kg/m^3 , ranging from $\sigma_\theta = 26.5$ – 27.5 kg/m^3 . The North Atlantic features the NADW with
251 salinity of 35 psu (Figure 5a) in the PI and MH, and expands through a large part of the
252 density parameter space. The GNAIW, which replaces the NADW in the LGM, shows a
253 minimum salinity of 36.3, and ranges from $\sigma_\theta = 28.5$ – 29.4 kg/m^3 .

3.2. Subduction rates calculations

254 The amount of water mass formation that departs the mixed layer downward across
255 the permanent pycnocline is measured by the annual subduction rate [*Cushman-Roisin*,
256 1987]. In the absence of interannual or shorter variability of the mixed layer, the fluid
257 leaving the mixed layer during the winter/spring time can irreversibly enter the permanent
258 thermocline [*Stommel*, 1979]. Here we use the same formulation of *Goes et al.* [2008] to
259 diagnose the annual subduction across the base of the ocean mixed layer as a function of
260 potential density at the region of the thermocline outcropping. According to *Goes et al.*
261 [2008] formulation, the annual subduction rate is calculated with respect to the maximum
262 annual mixed layer depth (H). The volume transfer of water subducted for each basin
263 as a function of density is obtained by integrating the positive values (downward) of the

264 Eulerian subduction rate, which is defined at each grid point, over the surface bounded
 265 by two adjacent isopycnals along H . This calculation is performed as follows:

$$Sub(\sigma_\theta) = - \oint_{\sigma_\theta - \frac{\Delta\sigma_\theta}{2}}^{\sigma_\theta + \frac{\Delta\sigma_\theta}{2}} [\mathbf{u}_H \cdot \nabla H + w_H] dA, \quad (1),$$

266 where the first term on right hand side of (1) represents the lateral induction across a
 267 sloping mixed layer base and the second term accounts for the vertical entrainment. In
 268 Equation (1), \mathbf{u}_H and w_H are the annual average of horizontal and vertical velocities,
 269 respectively, linearly interpolated to the annual maximum mixed layer depth H . The
 270 mixed layer depth is calculated following the criterion of *Large et al.* [1997], and H is
 271 the maximum winter time mixed layer depth, averaged over the last 20 years of model
 272 integration for each run. Density at the winter mixed layer is obtained from the averaged
 273 temperature and salinity fields, and interpolated to the depth H . The summations over
 274 the density intervals defined in (1) are divided into $\Delta\sigma_\theta = 0.2 \text{ kg/m}^3$ increments, and
 275 includes the regions comprised from the equator to 60° meridionally in each hemisphere.

276 Between 60°S and 60°N , the maximum H is found around the Labrador sea, reaching
 277 approximately 540 m in PI and MH, and over 1000 m in the LGM (not shown). Also in
 278 the LGM, the maximum H in the North Atlantic reaches further south ($\approx 40^\circ\text{N}$), which
 279 agrees with the southward migration of the zero wind stress curl in that period (Figure
 280 1), and with results from previous modeling studies [e.g., *Rahmstorf*, 2002; *Ganopolski*
 281 *et al.*, 1998].

282 In the considered regions of the Southern Hemisphere, the deepest mixed layer depths
 283 are located in the formation zones of the SAMW and AAIW, ranging from 100 m to

284 400 m. Changes between PI and MH are small, with differences of H generally below
285 10 m. Indeed, according to [Liu *et al.*, 2003], the wind stress changes have little impact
286 on the permanent thermocline in the mid-Holocene. In the LGM, increased wind stress
287 and wind stress curl in the Southern Ocean cause a broad thermocline deepening of 20
288 to 80 m there, since more water is downwelled from the mixed layer. No shift in the zero
289 wind stress curl line occurs among the climatic periods in the Southern ocean (Figure
290 1), and therefore no latitudinal migration of the deepest mixed layer depth and of the
291 position of the Subtropical Front [STF, *Stramma and Peterson*, 1990] is observed. It
292 should be noted that some previous studies [e.g., *Bard and Rickaby*, 2009; *Dickson et al.*,
293 2009; *Vázquez Riveiros et al.*, 2010] suggest a northward migration of the South Atlantic
294 STF for cooler stadials. Others suggest a southward migration of the STF [e.g., *Paul and*
295 *Schfer-Neth*, 2003] instead.

296 Figure 6 shows the transport of subducted waters for $25.0 < \sigma_\theta < 30.0 \text{ kg/m}^3$, for each
297 basin (divided in north and south sub-basins) and each climatic period. At lower densities
298 $\sigma_\theta < 26.0 \text{ kg/m}^3$, the subtropical waters, which are part of the shallow subtropical-cells.
299 At this range, subduction is highly driven by the vertical entrainment term (dashed lines
300 in Figure 6). MH and PI have similar formation rates in the southern Hemisphere in all
301 ocean basins. *Goes et al.* [2008] also show negligible changes in subduction transports
302 for the densities between $25.0 < \sigma_\theta < 25.8 \text{ kg/m}^3$ between the 20th and 21st century.
303 In the Northern hemisphere, changes between these two periods may be associated with
304 changes in the wind stress curl, since the ITCZ shifts northward in the MH simulation
305 [c.f., *Braconnot et al.*, 2007a]. In the LGM, there is a decrease in the subduction rates in

306 all densities in subtropical areas in the order of 2 Sv, especially in the Atlantic (Figure
307 6a). This is more consistent with the shrinkage of these lower density outcropping regions,
308 since there is a systematic increase of surface density during the LGM [*Billups and Schrag,*
309 2000]. The region located within the $26 < \sigma_\theta < 26.9 \text{ kg/m}^3$ range is largely associated with
310 the formation region for the mode waters in the PI and MH. In the Southern Hemisphere,
311 the SAMW formation is strongly tied to the formation of the AAIW. In the North Atlantic,
312 mode waters have a strong formation rate, and the subduction peaks in that region are
313 associated with formation of the subtropical mode water (STMW) and the denser subpolar
314 mode water (SPMW) and Labrador Sea Water [*Speer and Tziperman, 1992*]. In the North
315 Pacific (Figure 6b), which is less dense, this σ_θ range is associated with formation of the
316 NPIW [*Wong et al., 1999*]. In the LGM, these formation regions are generally shifted to
317 higher densities. The AAIW formation regions in the Southern Hemisphere ($26.9 < \sigma_\theta <$
318 27.4) show strong formation in the Indian and South Pacific basins, with a less extent in
319 the South Atlantic basin. Indeed previous studies show that half of the AAIW formation
320 occurs in the South Pacific [*Downes et al., 2010; Karstensen and Quadfasel, 2002*].

321 In the LGM, a strong peak is observed in the North Atlantic associated with the glacial
322 AAIW water mass at $\sigma_\theta > 28.5 \text{ kg/m}^3$, which is observed as a salinity minimum in the θ -S
323 diagram (Figure 5b). This peak indicates vigorous water mass formation at this density
324 class, at the expense of a deeper NADW formation in the Nordic Seas [e.g., *Curry and*
325 *Oppo, 2005; Oppo and Fairbanks, 1987*]. The AAIW ventilation is restricted to the lower
326 depths as seen in the section profile of Figures 3 and 4.

327 The sum of subducted waters of SAMW and AAIW classes (Table 1), taking into
328 account the different density ranges between the LGM and PI/MH, shows that there is a
329 2 Sv (20 %) increase of subduction of intermediate waters in the South Atlantic for the
330 MH, and 2 Sv (about 40 %) decrease in the North Atlantic, when comparing to PI. An
331 increase of the same magnitude is seen in the Pacific MH AAIW/SAMW formation of
332 about 2 Sv in both northern and southern basins. In the Indian ocean negligible variability
333 is seen in the SAMW/AAIW formation within the $\sigma_\theta = 26.4\text{--}27.5$ kg/m³ range, with 12.0
334 Sv for the PI and 12.2 Sv for the MH. The overall characteristic in CCSM3 during the
335 LGM is a shift to higher densities during for all basins of about $\Delta\sigma_\theta = 1\text{--}1.3$ kg/m³. This
336 is similar but with opposite sign of results from *Goes et al.* [2008] for a warmer climate.
337 Also, except for the North Pacific, which show the same rate of NPIW formation of about
338 10 Sv, there is a general increase from 50 % up to 100 % of AAIW/SAMW formation
339 in the LGM. The increased subduction in the North Atlantic, South Pacific and Indian
340 basins at intermediate waters are able to replace the lack of deep water formation in those
341 regions, and the low difference in the Atlantic meridional overturning circulation strength
342 (c.f. *Otto-Bliesner et al.* [2006]) confirms this result.

4. Discussion and Conclusions

343 In the LGM, the main changes observed in the water mass formation are consistent
344 with an intensification of the Southern Hemisphere overturning due to enhanced AABW
345 formation. In addition, there is a 0.2-0.4 dyne/cm² increase in the SHZW occurs during
346 the LGM relative to the PI.

347 The formation and circulation of the AAIW is an important component of the upper
348 branch of the meridional overturning circulation that is associated with the transport of
349 heat and salt within the Southern Hemisphere subtropical gyre [*Schmitz, 1996; Sloyan*
350 *and Rintoul, 2001; Talley, 2003*]. The AABW mostly forms in the Ross and Weddell
351 Seas, spreading below NADW, and is associated with the lower branch of the MOC. Its
352 formation is due to, among other things, a combination of sea-ice /ice-shelf melt and brine
353 rejection. Therefore sea-ice changes in the Southern Ocean have a significant role in the
354 modulation of changes in the oceans meridional overturning [*Goosse and Fichefet, 1999;*
355 *Shin et al., 2003a*].

356 With the increased sea-ice formation and expansion at the LGM, there is an associated
357 increase in the surface density flux off Antarctica in the Southern Oceans [*Shin et al.,*
358 *2003b, a; Clauzet et al., 2007*] causing deep circulation changes (i.e. enhanced AABW).
359 As discussed by *Duplessy et al. [1988]; Liu et al. [2003]* paleoclimate records also suggest
360 a shallower and weaker NADW circulation and an enhanced AABW intrusion into the
361 North Atlantic at LGM accompanied by intensification of westerly winds and AAIW
362 production. In fact, *McKay et al. [2012]* discuss, in the context of the late Pliocene
363 cooling, how the intensification of Southern Hemisphere westerly winds are associated
364 with a more vigorous ocean circulation and have been linked to increased production of
365 AAIW at the LGM [*Muratli et al., 2009*].

366 Stronger SHZW is associated with enhanced northward Ekman transport which inten-
367 sifies the AAIW. Previous work shows through several numerical experiments in an ocean
368 general circulation model, that the production of AAIW is dependent on the strength of

369 the Southern Hemisphere winds *Ribbe* [2001]. AAIW changes in ventilation have been
370 associated with Ekman heat and freshwater transport changes caused by wind stress
371 variability in the Southern Ocean [e.g., *Rintoul and England*, 2002; *Sallee et al.*, 2006;
372 *Naveira Garabato et al.*, 2009].

373 Many studies propose that the SHZW may move equatorward and perhaps weaken
374 during glacial periods [e.g., *Toggweiler et al.*, 2006; *Bard and Rickaby*, 2009; *Dickson*
375 *et al.*, 2009; *Vázquez Riveiros et al.*, 2010], both of which would reduce the northward
376 export of Antarctic surface waters and the resulting upwelling of relatively salty deep
377 water. An increase in the Southern Ocean upwelling during Northern Hemisphere cold
378 intervals is consistent with several paleodata studies [e.g., *Anderson et al.*, 2009; *Skinner*
379 *et al.*, 2010; *Spero and Lea*, 2002] synthesized by *Denton et al.* [2010].

380 They suggest that climate-related shifts in the mean position of the Southern Hemi-
381 sphere westerlies can be inferred from different sources of paleo-proxy data. Recent model-
382 ing results point to a link between Northern Hemisphere cooling and SHZW strengthening
383 via a shift in the Intertropical Convergence Zone and the resulting effects on the Hadley
384 circulation [*Lee et al.*, 2011]. Also, recent analysis of benthic foraminiferal Cd/Ca by
385 *Makou et al.* [2010] suggest, much in agreement with the results shown in Figure 3, that
386 the AAIW was unique to the glacial South Atlantic and that it formed differently than
387 today.

388 During the MH, the fresher North Atlantic shows reduced subduction in intermediate
389 levels by 2 Sv, but increased AAIW formation by 2 Sv. In the Pacific, there is an in-
390 crease of subduction in the MH for both AAIW and NPIW of 2.7 Sv, but mostly due to

391 enhanced AAIW (2 Sv). In the LGM, both AAIW and GNAIW increase (4.2 and 5.3 Sv,
392 respectively), meaning that both southern and northern intermediate waters contribute
393 to replacing the lack of NADW in the LGM.

394 In CCSM3, the increase of AAIW formation in the South Pacific and Indian Oceans
395 does not represent increased ventilation in deep levels, since the AABW and PDW are
396 much denser, presumably due to excess ice formation in the CCSM, and the deep ocean
397 is more stagnant (as discussed in *Shin et al. [2003a]*; *Liu et al. [2005]*).

398 Less upwelling of old waters would increase the carbon concentration of the deep ocean.
399 This is consistent with *Skinner et al. [2010]* who found much older deep water circula-
400 tion around Antarctica during the last glacial period. This relatively coarse resolution
401 version of the CCSM3 can not simulate eddies, which are parameterized by the Gent and
402 McWilliams diffusion. Increased mixing by eddies in response to strengthened winds in
403 the polar regions could counteract the increased Ekman transport [*Meredith and Hogg,*
404 2006], and therefore reduce the wind-driven response during the LGM.

405 **Acknowledgments.**

406 This work was supported in part by grants from FAPESP, CNPq-300223/93-5 and
407 CNPq-MCT-INCT-Criosfera. Marlos Goes carried out this research under the auspices
408 of the Cooperative Institute for Marine and Atmospheric Studies (CIMAS), a cooper-
409 ative institute of the University of Miami and the National Oceanic and Atmospheric
410 Administration, cooperative agreement # NA17RJ1226.

References

- 411 Adkins, J., K. McIntyre, and D. Schrag, The salinity, temperature, and $\delta^{18}\text{O}$ of the
412 glacial deep ocean, *Science*, *298*(5599), 1769–1773, 2002.
- 413 Anderson, R., S. Ali, L. Bradtmiller, S. Nielsen, M. Fleisher, B. Anderson, and L. Bur-
414 ckle, Wind-driven upwelling in the southern ocean and the deglacial rise in atmo-
415 spheric CO_2 , *Science*, *323*(5920), 1443–1448, doi:10.1126/science.1167441, 2009.
- 416 Bard, E., and R. Rickaby, Migration of the subtropical front as a modulator of glacial
417 climate, *Nature*, *460*(7253), 380–383, 2009.
- 418 Billups, K., and D. P. Schrag, Surface ocean density gradients during the Last Glacial
419 Maximum, *Paleoceanography*, *15*, 110–123, 2000.
- 420 Braconnot, P., et al., Results of PMIP2 coupled simulations of the mid-holocene and
421 last glacial maximum – Part 1: Experiments and large-scale features, *Clim. Past*, *3*,
422 261277, 2007a.
- 423 Braconnot, P., et al., Results of PMIP2 coupled simulations of the mid-holocene and
424 last glacial maximum – Part 2: Feedbacks with emphasis on the location of the itcz
425 and mid- and high latitudes heat budget, *Clim. Past*, *3*, 279296, 2007b.
- 426 Briegleb, B., C. Bitz, E. Hunke, W. Lipscomb, M. Holland, J. Schramm, and R. Moritz,
427 Scientific description of the sea ice component in the community climate system model,
428 version three, *NCAR Technical Note NCAR/TN-463+ STR*, 2004.
- 429 Clauzet, G., I. Wainer, A. Lazar, E. Brady, and B. Otto-Bliesner, A numerical study of
430 the south Atlantic circulation at the last glacial maximum, *Palaeogeography, Palaeo-*
431 *climatology, Palaeoecology*, *253*(3-4), 509–528, 2007.

- 432 Clauzet, G., I. Wainer, and M. Bicego, Validating NCAR-CCSM last glacial maximum
433 sea surface temperature in the tropical and south Atlantic with proxy-data, *Palaeo-*
434 *geography, Palaeoclimatology, Palaeoecology*, 267(3-4), 153–160, 2008.
- 435 Cleroux, C., P. deMenocal, and T. Guilderson, Deglacial radiocarbon history of tropical
436 Atlantic thermocline waters: absence of CO₂ reservoir purging signal, *Quaternary*
437 *Science Reviews*, 30, 1875–1882, 2011.
- 438 Collins, W., et al., The formulation and atmospheric simulation of the community at-
439 mosphere model: CAM3, *J. Climate*, 19(11), 2144–2161, 2006.
- 440 Curry, W. B., and D. W. Oppo, Glacial water mass geometry and the distribution
441 of D13C of σ CO₂ in the western atlantic ocean, *Paleoceanography*, 20, PA1017, doi:
442 10.1029/2004PA001021, 2005.
- 443 Cushman-Roisin, B., Subduction, *Hawaii Univ, Dynamics of the Oceanic Surface Mixed*
444 *Layer p 181-196(SEE N 88-20785 13-48)*, 1987.
- 445 Daellenbach, A., T. Blunier, J. Flückiger, B. Stauffer, J. Chappellaz, and D. Raynaud,
446 Changes in the atmospheric CH₄ gradient between Greenland and Antarctica during
447 the Last Glacial and the transition to the Holocene, *Geophysical Research Letters*, 27,
448 1005, 2000.
- 449 Denton, G., R. Anderson, J. Toggweiler, R. Edwards, J. Schaefer, and A. Putnam, The
450 last glacial termination, *Science*, 328(5986), 1652, 2010.
- 451 Dickinson, R., K. Oleson, G. Bonan, F. Hoffman, P. Thornton, M. Vertenstein, Z. Yang,
452 and X. Zeng, The community land model and its climate statistics as a component of
453 the community climate system model, *Journal of Climate*, 19(11), 2302–2324, 2006.

- 454 Dickson, A., C. Beer, C. Dempsey, M. Maslin, J. Bendle, E. McClymont, and R. Pancost,
455 Oceanic forcing of the marine isotope stage 11 interglacial, *Nature Geoscience*, *2*(6),
456 428–433, 2009.
- 457 Downes, S. M., N. L. Bindoff, and S. R. Rintoul, Changes in the subduction of Southern
458 Ocean water masses at the end of the twenty-first century in eight IPCC models, *J.*
459 *Climate*, *23*, 6526–6541, doi:<http://dx.doi.org/10.1175/2010JCLI3620.1>, 2010.
- 460 Drijfhout, S. S., J. Donners, and W. P. M. de Ruijter, The origin of intermediate and
461 subpolar mode waters crossing the Atlantic equator in OCCAM, *Geophys. Res. Lett.*,
462 *32*, L06602, doi:doi:10.1029/2004GL021851, 2005.
- 463 Duplessy, J., N. Shackleton, R. Fairbanks, L. Labeyrie, D. Oppo, and N. Kallel, Deep-
464 water source variations during the last climatic cycle and their impact on the global
465 deepwater circulation, *Paleoceanography*, *3*(3), 343–360, 1988.
- 466 Fischer, H., J. Schmitt, D. Luthi, T. Stocker, T. Tschumi, P. Parekh, F. Joos, P. Köhler,
467 et al., The role of southern ocean processes in orbital and millennial CO₂ variations-a
468 synthesis, *Quaternary Science Reviews*, *29*(1-2), 193–205, 2010.
- 469 Flückiger, J., A. Dällenbach, T. Blunier, B. Stauffer, T. Stocker, D. Raynaud, and
470 J. Barnola, Variations in atmospheric N₂O concentration during abrupt climatic
471 changes, *Science*, *285*(5425), 227, 1999.
- 472 Ganopolski, A., S. Rahmstorf, V. Petoukhov, and M. Claussen, Simulation of modern
473 and glacial climates with a coupled global model of intermediate complexity, *Nature*,
474 *391*, 351–356, 1998.

- 475 Gent, P., F. Bryan, G. Danabasoglu, K. Lindsay, D. Tsumune, M. Hecht, and S. Doney,
476 Ocean chlorofluorocarbon and heat uptake during the twentieth century in the
477 CCSM3, *Journal of Climate*, 19(11), 2366–2381, 2006.
- 478 Goes, M., I. Wainer, P. R. Gent, and F. O. Bryan, Changes in subduction in the South
479 Atlantic Ocean during the 21st century in the CCSM3, *Geophysical Res. Letters*, 35,
480 L6701, doi:10.1029/2007GL032762, 2008.
- 481 Goosse, H., and T. Fichefet, Importance of ice-ocean interactions for the global ocean
482 circulation: A model study, *Journal of Geophysical Research*, 104(C10), 23,337–23,355,
483 1999.
- 484 Herguera, J., T. Herbert, M. Kashgarian, and C. Charles, Intermediate and deep water
485 mass distribution in the Pacific during the last glacial maximum inferred from oxygen
486 and carbon stable isotopes, *Quaternary Science Reviews*, 29(9), 1228–1245, 2010.
- 487 Joyce, T., J. Luyten, A. Kubryakov, F. Bahr, and J. Pallant, Meso-to large-scale struc-
488 ture of subducting water in the subtropical gyre of the eastern North Atlantic ocean,
489 *Journal of physical oceanography*, 28(1), 40–61, 1998.
- 490 Karstensen, J., and D. Quadfasel, Formation of southern hemisphere thermocline waters:
491 Water mass conversion and subduction, *Journal of Physical Oceanography*, 32(11),
492 3020–3038, 2002.
- 493 Large, W. G., G. Danabasoglu, S. C. Doney, and J. C. McWilliams, Sensitivity to
494 surface forcing and boundary layer mixing in a global ocean model: Annual-mean
495 climatology, *J. Phys. Oceanogr.*, 27, 2418–2447, 1997.

- 496 Lee, S.-Y., J. C. H. Chiang, K. Matsumoto, and K. S. Tokos, Southern ocean wind
497 response to North Atlantic cooling and the rise in atmospheric CO₂: Modeling
498 perspective and paleoceanographic implications, *Paleoceanography*, *26*, PA1214, doi:
499 doi:10.1029/2010PA002004, 2011.
- 500 Liu, Z., Glacial thermohaline circulation and climate: Forcing from the north or south?,
501 *Advances in Atmospheric Sciences*, *23*(2), 199–206, 2006.
- 502 Liu, Z., I. Kutzbach, and L. Wu, Modelling climate shift of El Nino variability in the
503 holocene, *Geophysical Research Letters*, *27*(15), 2265–2268, 2000.
- 504 Liu, Z., E. Brady, and J. Lynch-Stieglitz, Global ocean response to orbital forcing in
505 the holocene, *Paleoceanography*, *18*(2), 1041, 2003.
- 506 Liu, Z., S. Shin, R. Webb, W. Lewis, and B. Otto-Bliesner, Atmospheric CO₂ forcing
507 on glacial thermohaline circulation and climate, *Geophys. Res. Lett*, *32*(2), L02,706,
508 2005.
- 509 Makou, M., D. Oppo, and W. Curry, South Atlantic intermediate water mass geometry
510 for the last glacial maximum from foraminiferal cd/ca, *Paleoceanography*, *25*(4), 2010.
- 511 Marchitto, T., and W. Broecker, Deep water mass geometry in the glacial Atlantic
512 ocean: A review of constraints from the paleonutrient proxy Cd, *Geochem. Geophys.*
513 *Geosyst*, *7*, Q12,003, 2006.
- 514 Matsumoto, K., T. Oba, J. Lynch-Stieglitz, and H. Yamamoto, Interior hydrography
515 and circulation of the glacial Pacific ocean, *Quat. Sci. Rev.*, *21*, 1693–1704, 2002.
- 516 McCartney, M. S., Subantarctic Mode Water, *A voyage of Discovery*, *24*, 103–119, 1977.

- 517 McKay, R., et al., Antarctic and Southern Ocean influences on Late Pliocene global
518 cooling, *Proceedings of the National Academy of Sciences*, 2012.
- 519 McNeil, B., R. Matear, R. Key, J. Bullister, and J. Sarmiento, Anthropogenic CO₂ up-
520 take by the ocean based on the global chlorofluorocarbon data set, *Science*, 299(5604),
521 235, 2003.
- 522 Meredith, M. P., and A. M. Hogg, Circumpolar response of southern ocean eddy activity
523 to a change in the southern annular mode, *Geophys. Res. Lett.*, 33, L16,608, 2006.
- 524 Monnin, E., A. Indermühle, A. Dällenbach, J. Flückiger, B. Stauffer, T. Stocker, D. Ray-
525 naud, and J. Barnola, Atmospheric CO₂ concentrations over the last glacial termina-
526 tion, *Science*, 291(5501), 112, 2001.
- 527 Muratli, J., Z. Chase, A. Mix, and J. McManus, Increased glacial-age ventilation of the
528 Chilean margin by antarctic intermediate water, *Nature Geoscience*, 2009.
- 529 Naveira Garabato, A., L. Jullion, D. Stevens, K. Heywood, and B. King, Variability
530 of subantarctic mode water and antarctic intermediate water in the Drake passage
531 during the late-twentieth and early-twenty-first centuries, *Journal of Climate*, 22(13),
532 3661–3688, 2009.
- 533 Oppo, D., and R. Fairbanks, Variability in the deep and intermediate water circulation
534 of the Atlantic ocean during the past 25,000 years: Northern Hemisphere modulation
535 of the Southern Ocean, *Earth and Planetary Science Letters*, 86(1), 1–15, 1987.
- 536 Otto-Bliesner, B., E. Brady, G. Clauzet, R. Tomas, S. Levis, and Z. Kothavala, Last
537 glacial maximum and holocene climate in CCSM3, *Journal of Climate*, 19(11), 2526–
538 2544, 2006.

- 539 Otto-Bliesner, B., C. Hewitt, T. Marchitto, E. Brady, A. Abe-Ouchi, M. Crucifix, S. Mu-
540 rakami, and S. Weber, Last glacial maximum ocean thermohaline circulation: PMIP2
541 model intercomparisons and data constraints, *Geophys Res Lett*, *34*, 2007.
- 542 Otto-Bliesner, B., et al., A comparison of PMIP2 model simulations and the margo
543 proxy reconstruction for tropical sea surface temperatures at last glacial maximum,
544 *Climate dynamics*, *32*(6), 799–815, 2009.
- 545 Pahnke, K., and R. Zahn, Southern hemisphere water mass conversion linked with North
546 Atlantic climate variability, *Science*, *307*(5716), 1741, 2005.
- 547 Pahnke, K., S. Goldstein, and S. Hemming, Abrupt changes in antarctic intermediate
548 water circulation over the past 25,000 years, *Nature Geoscience*, *1*(12), 870–874, 2008.
- 549 Paul, A., and C. Schfer-Neth, Modeling the water masses of the Atlantic ocean at the last
550 glacial maximum, *Paleoceanography*, *18*(3), 1058, doi:10.1029/2002PA000783., 2003.
- 551 Peltier, W. R., Global glacial isostasy and the surface of the ice-age earth: The ICE-5G
552 (VM2) model and GRACE, *Annu. Rev. Earth Planet. Sci.*, *32*, 111149, 2004.
- 553 Rahmstorf, S., Ocean circulation and climate during the past 120,000 years, *Nature*,
554 *419*, 207–214, 2002.
- 555 Ribbe, J., Intermediate water mass production controlled by Southern Hemisphere
556 winds, *Geophysical research letters*, *28*(3), 535–538, 2001.
- 557 Rintoul, S., and M. England, Ekman transport dominates local air-sea fluxes in driving
558 variability of subantarctic mode water, *Journal of physical oceanography*, *32*(5), 1308–
559 1321, 2002.

- 560 Sabine, C., and T. Tanhua, Estimation of anthropogenic CO₂ inventories in the ocean,
561 *Annual Review of Marine Science*, *2*, 175–198, 2010.
- 562 Sabine, C., et al., The oceanic sink for anthropogenic CO₂, *Science*, *305*(5682), 367,
563 2004.
- 564 Sallee, J., N. Wienders, K. Speer, and R. Morrow, Formation of subantarctic mode
565 water in the southeastern Indian ocean, *Ocean Dynamics*, *56*(5), 525–542, 2006.
- 566 Schmitz, J., W. J., *On the World Ocean Circulation*, The Pacific and Indian Oceans/A
567 global update. Tech. Rep. WHOI-96-08,, 1996.
- 568 Shin, S., Z. Liu, B. Otto-Bliesner, E. Brady, J. Kutzbach, and S. Harrison, A simulation
569 of the Last Glacial Maximum climate using the NCAR-CCSM, *Climate Dynamics*,
570 *20*(2), 127–151, 2003a.
- 571 Shin, S., Z. Liu, B. Otto-Bliesner, J. Kutzbach, and S. Vavrus, Southern ocean sea-
572 ice control of the glacial North Atlantic thermohaline circulation, *Geophys. Res. Lett*,
573 *30*(2), 1096, 2003b.
- 574 Skinner, L., S. Fallon, C. Waelbroeck, E. Michel, and S. Barker, Ventilation of the
575 deep southern ocean and deglacial CO₂ rise, *Science*, *328*(5982), 1147–1151, doi:
576 10.1126/science.1183627, 2010.
- 577 Sloyan, B., and S. Rintoul, Circulation, renewal, and modification of antarctic mode
578 and intermediate water, *Journal of physical oceanography*, *31*(4), 1005–1030, 2001.
- 579 Sloyan, B. M., and I. V. Kamenkovich, Simulation of subantarctic mode and antarctic
580 intermediate waters in climate models, *Journal of Climate*, *20*(20), 5061–5080, doi:
581 DOI 10.1175/JCLI4295.1, 2007.

- 582 Sørensen, J. V. T., J. Ribbe, and G. Shaffer, Antarctic Intermediate Water Mass For-
583 mation in Ocean General Circulation Models, *Journal of Physical Oceanography*, *31*,
584 3295–3311, doi:10.1175/1520-0485(2001)031, 2001.
- 585 Speer, K., and E. Tziperman, Rates of water mass formation in the North Atlantic,
586 *Journal of Physical Oceanography*, *22*, 93–104, 1992.
- 587 Spero, H., and D. Lea, The cause of carbon isotope minimum events on glacial termi-
588 nations, *Science*, *296*(5567), 522–525, 2002.
- 589 Stommel, H., Determination of Water Mass Properties of Water Pumped down from the
590 Ekman Layer to the Geostrophic Flow below, *Proceedings of the National Academy of*
591 *Science*, *76*, 3051–3055, 1979.
- 592 Stramma, L., and R. Peterson, The South Atlantic Current, *Journal of Physical Oceanog-*
593 *raphy*, *20*(6), 846–859, 1990.
- 594 Taft, B. A., Distribution of salinity and dissolved oxygen on surfaces of uniform potential
595 specific volume in the south Atlantic, south Pacific and Indian oceans, *J. Mar. Res.*,
596 *21*, 129146, 1963.
- 597 Talley, L., Distribution and formation of North Pacific intermediate water, *Journal of*
598 *Physical Oceanography*, *23*, 517–517, 1993.
- 599 Talley, L., *Antarctic Intermediate Water in the South Atlantic*, The South Atlantic:
600 Present and Past Circulation, G. Wefer et al., Eds., Springer Verlag, 219–238, 1996.
- 601 Talley, L., Some aspects of ocean heat transport by the shallow, intermediate and deep
602 overturning circulations, *Geophysical Monograph (American Geophysical Union)*, *112*,
603 1–22, 1999.

- 604 Talley, L., Shallow, intermediate, and deep overturning components of the global heat
605 budget, *Journal of Physical Oceanography*, *33*(3), 530–560, 2003.
- 606 Toggweiler, J., Variation of atmospheric CO₂ by ventilation of the ocean’s deepest water,
607 *Paleoceanography*, *14*(5), 571–588, doi:doi:10.1029/1999PA900033., 1999.
- 608 Toggweiler, J., J. Russell, and S. Carson, Midlatitude westerlies, atmospheric CO₂, and
609 climate change during the ice ages, *Paleoceanography*, *21*(2), 1–A2005, 2006.
- 610 Vázquez Riveiros, N., C. Waelbroeck, L. Skinner, D. Roche, J. Duplessy, and E. Michel,
611 Response of South Atlantic deep waters to deglacial warming during terminations V
612 and I, *Earth and Planetary Science Letters*, *298*(3-4), 323–333, 2010.
- 613 Wong, A., N. Bindoff, and J. Church, Large-scale freshening of intermediate waters in
614 the Pacific and Indian oceans, *Nature*, *400*(6743), 440–443, 1999.

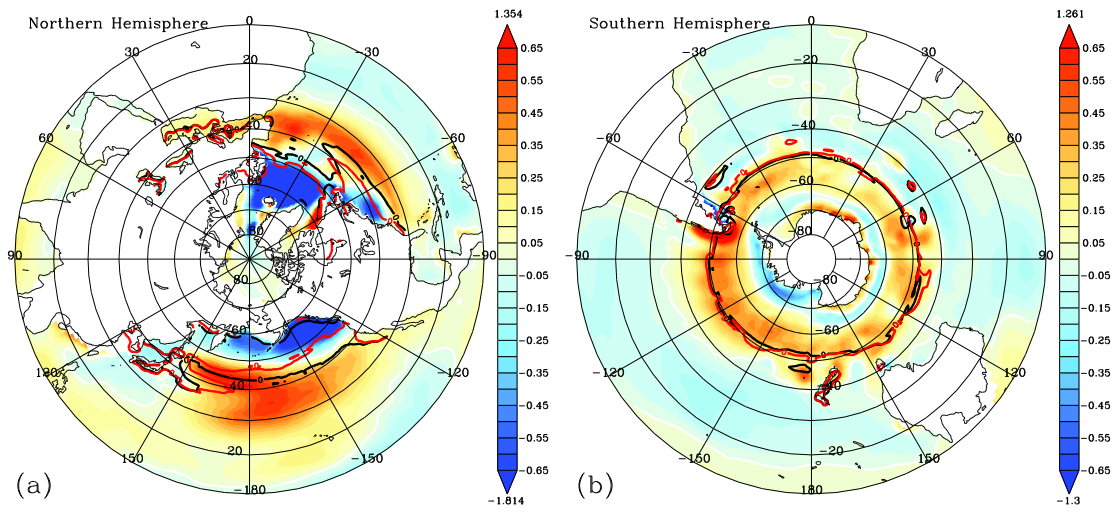


Figure 1. Difference field (LGM - PI) for (a) Northern and (b) Southern Hemisphere Zonal wind stress (NHZW and SHZW, respectively) in dyne/cm^2 . Also shown are the positions of zero wind stress curl for the LGM (black contours) and PI (red contours). The LGM winds are more intense by 0.2-0.4 (dyne/cm^2) in the south.

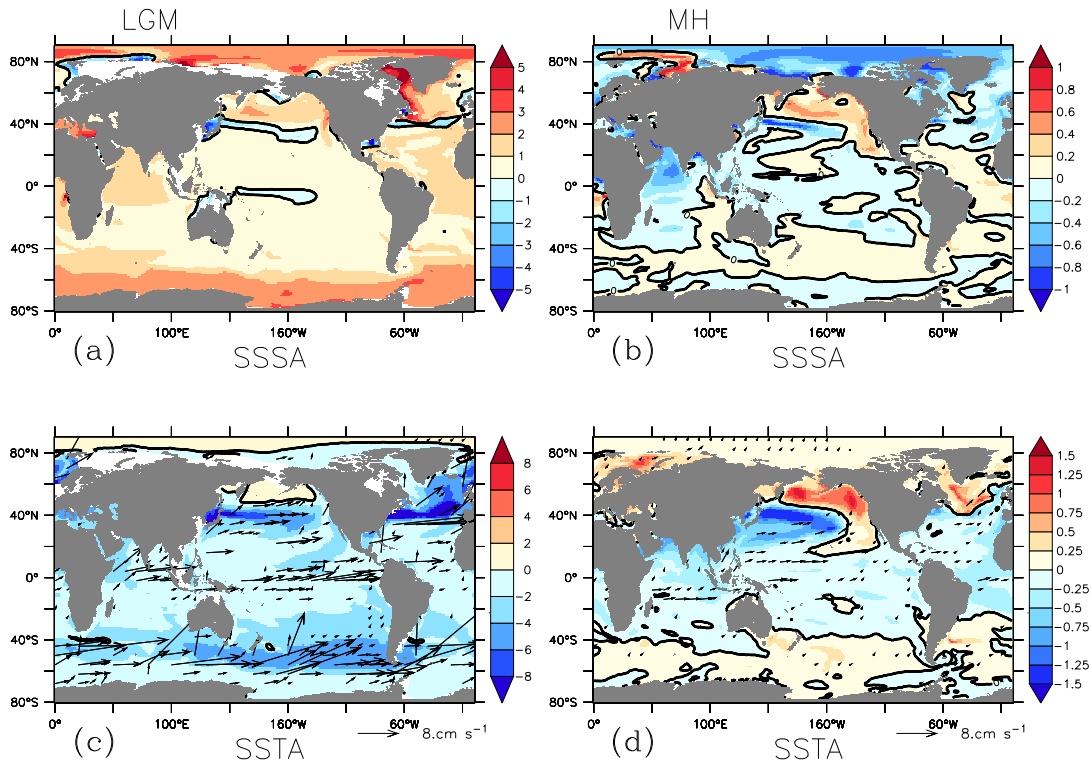


Figure 2. Global annual sea surface salinity (SSSA) and temperature (SSTA) differences relative to PI for the LGM (a, c) and MH (b, d). Average annual velocity differences in the upper 80 m of the ocean are overlaid on the temperature panels for the respective periods. Only velocity differences about 1 cm/s are displayed

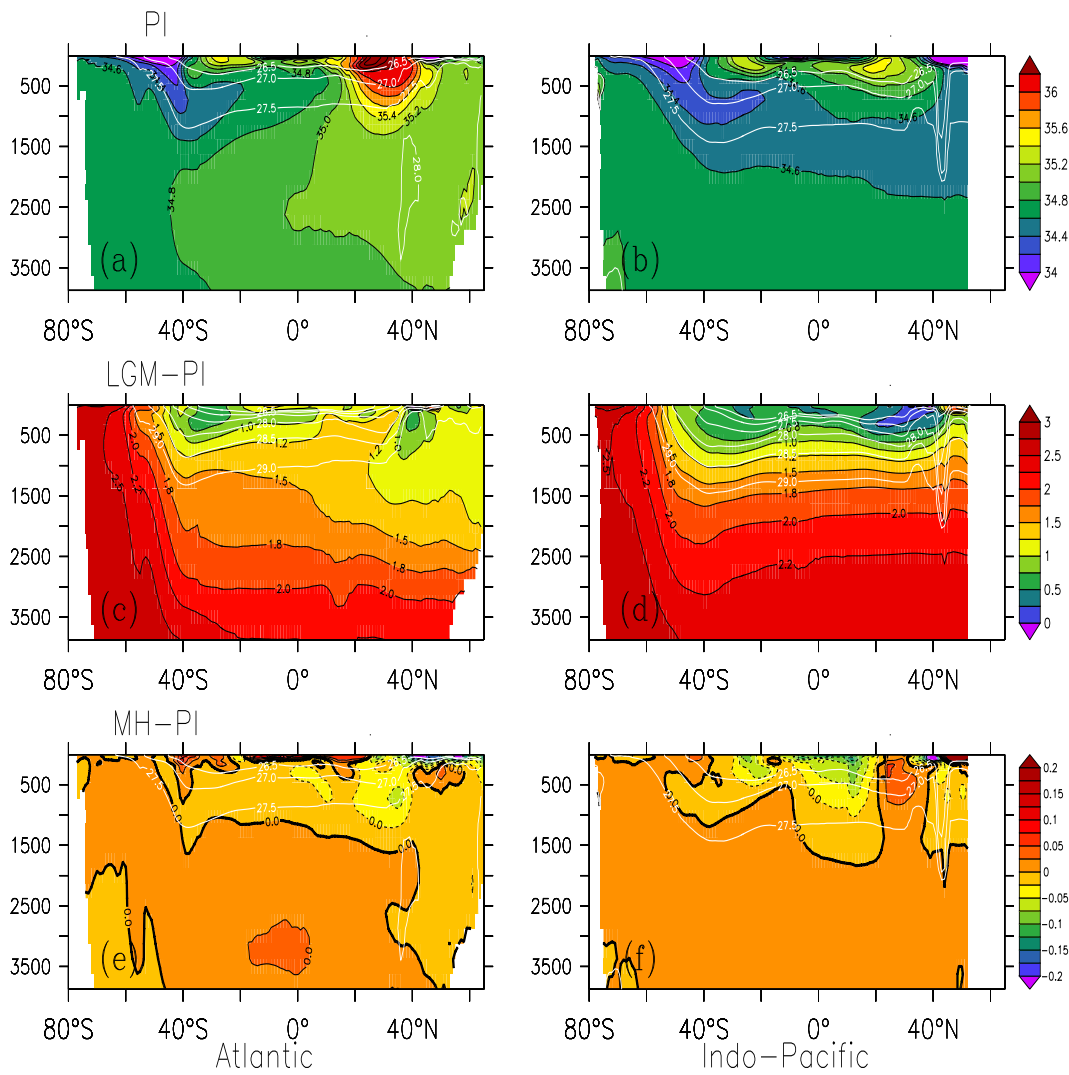


Figure 3. Zonal average salinity (psu) for the PI in the (a) Atlantic and (b) Indo-Pacific basins. Salinity differences relative to PI for the LGM (c, d) and MH (e, f), with the respective PI panel positions for the Atlantic (left) and Indo-Pacific (right) basins. Zonal average potential density contours (kg m^{-3}) are overlaid in white for each basin and geological period.

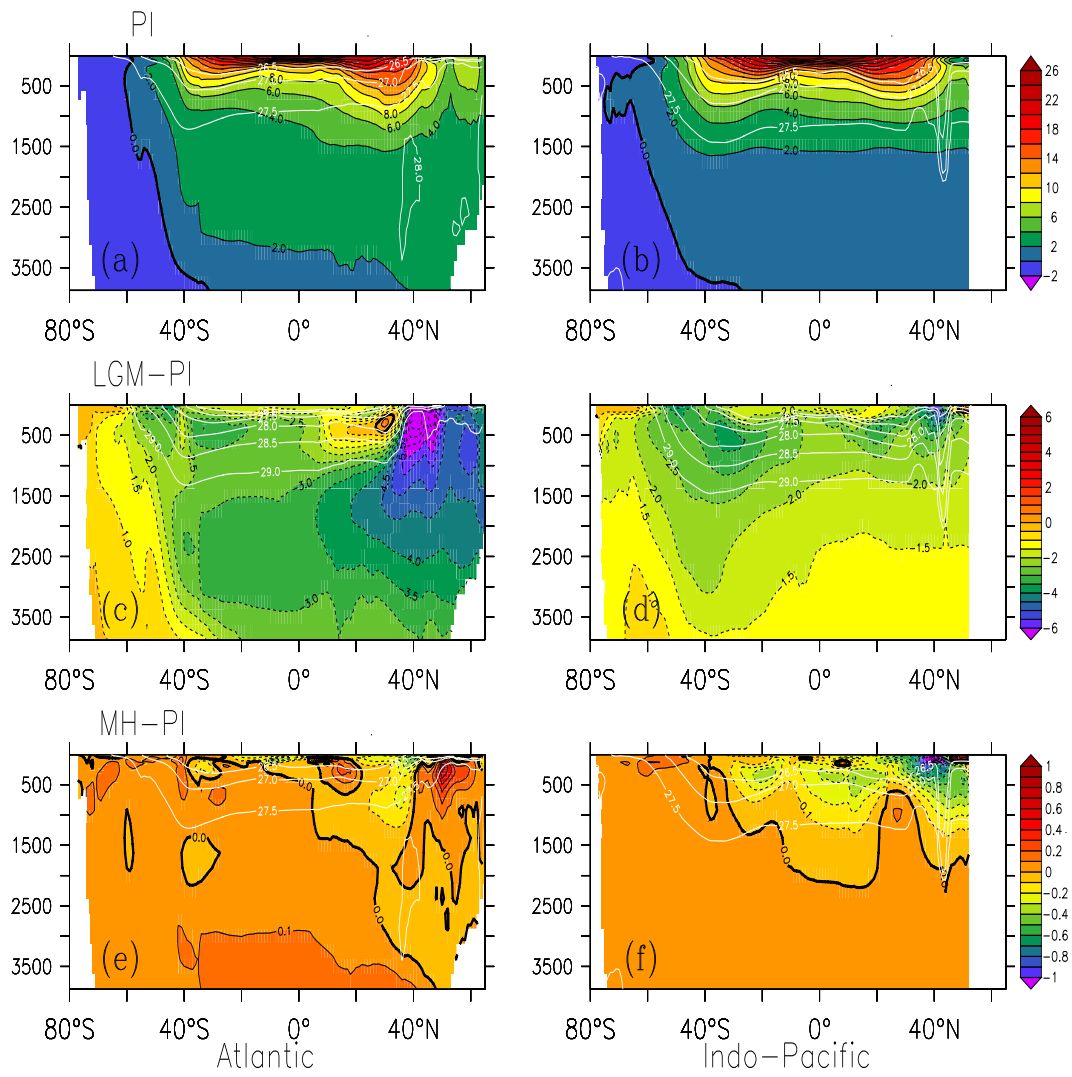


Figure 4. Same as Figure 3 but for potential temperature (°C).

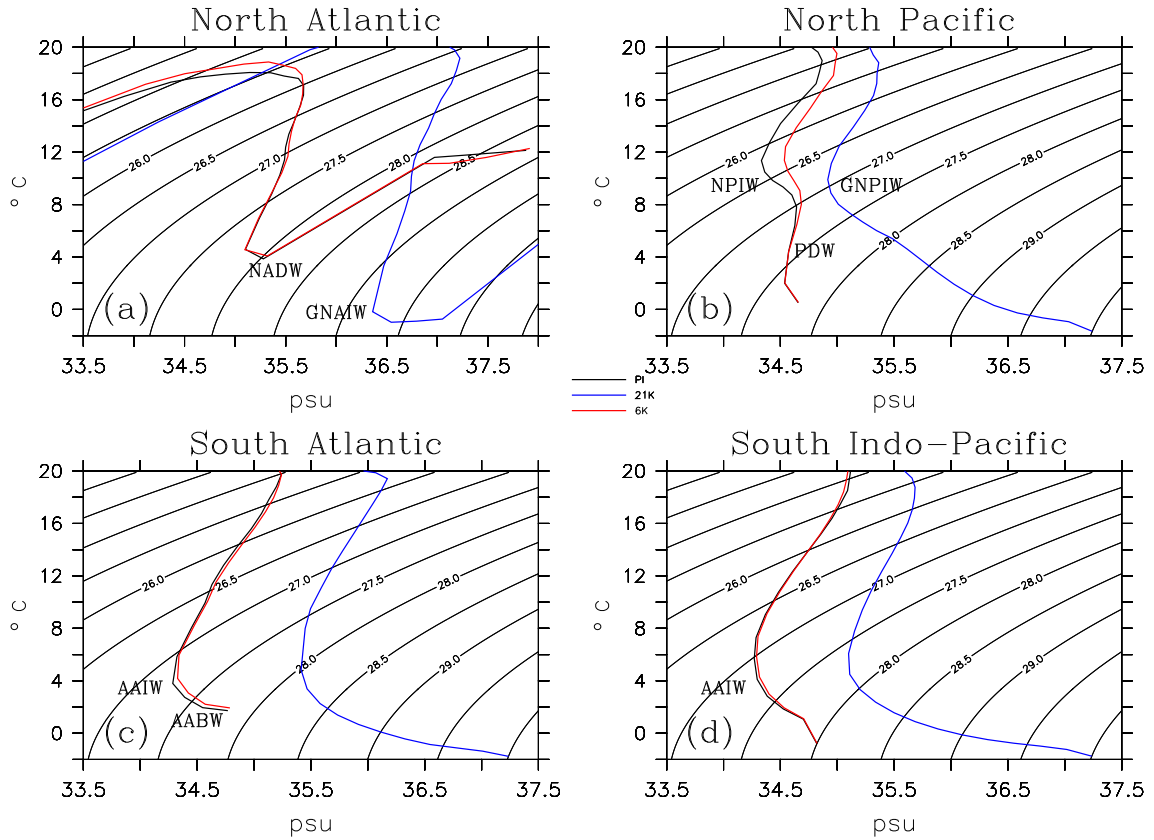


Figure 5. Mean potential temperature versus salinity (θ / S) diagrams for full-depth profiles averaged for Pre-Industrial (PI, black), Mid-Holocene (MH, red) and LGM (blue) simulations for (a) North Atlantic, (b) North Pacific, (c) South Atlantic, and (d) South Indo-Pacific. Basins averages are defined between 15° and 60° of latitude. Isopycnals (σ_θ , kg/m^3) are also shown. The position of the main water masses are included: Antarctic Intermediate Water (AAIW); Antarctic Bottom Water (AABW); North Atlantic Deep Water (NADW); North Pacific Intermediate Water (NPIW); Pacific Deep Water (PDW).

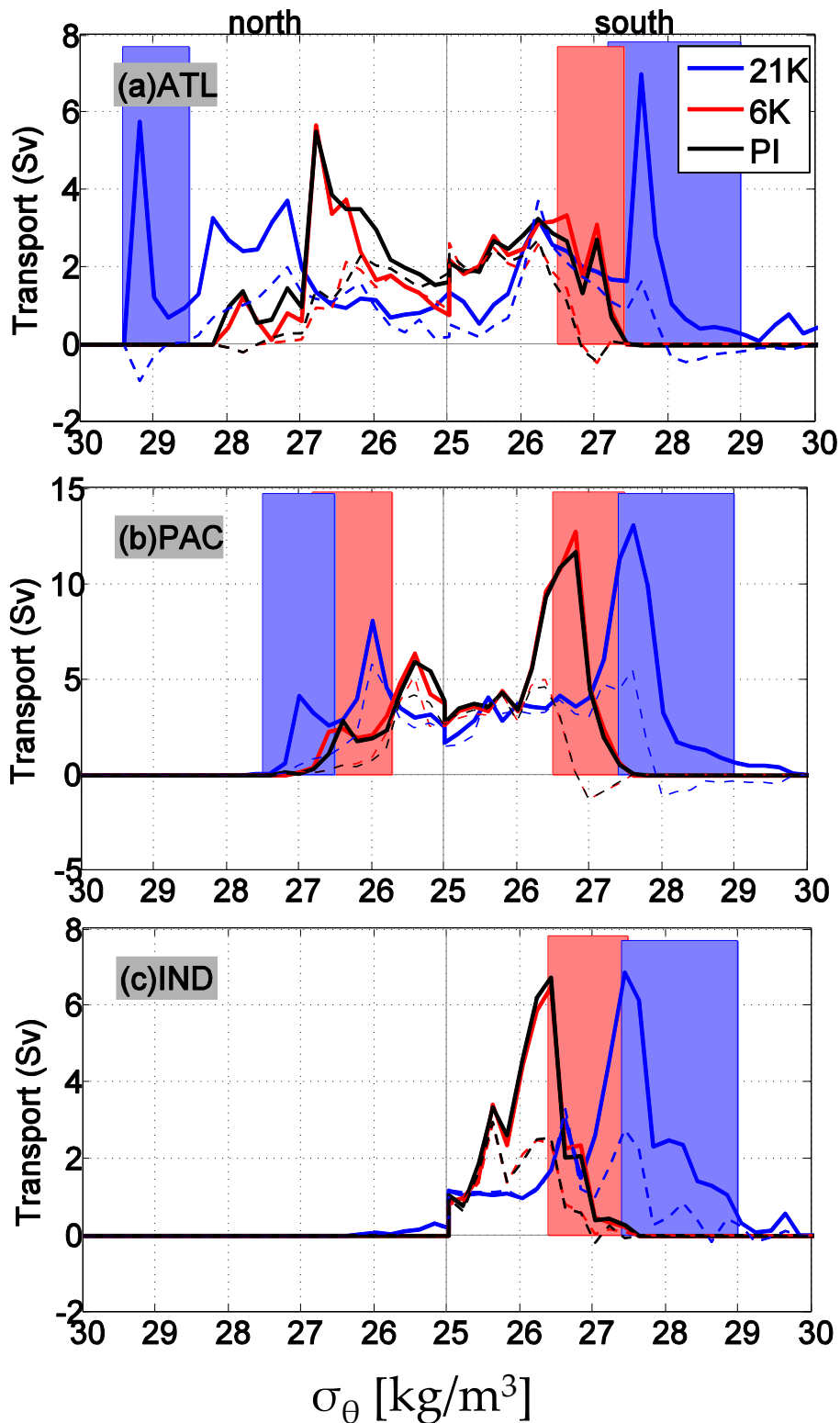


Figure 6. Transport (Sv) of subducted waters as a function of potential density σ_θ (kg m^{-3}) for the a) Atlantic, b) Pacific, and c) Indian Oceans on each climatic period (black curve=PI; red curve=MH and blue curve=LGM). The vertical entrainment component of the subduction is plotted as dashed lines. The potential density range of the intermediate and the densest mode waters are shaded with the period respective color. Note that the black and red shaded areas are overlapped, since the PI and MH share similar subduction regions

D R A F T

May 29, 2012, 10:52am.

D R A F T

Table 1. Transport (Sv) of subducted waters (Sub) showing the σ_θ range (kg m^{-3}) of the intermediate/mode waters for each basin and time period.

Simulation		Atlantic		Pacific		Indian
		south	north	south	north	south
PI	Sub	10.4	5.8	29.4	10.2	12.0
	σ_θ	26.5 – 27.4	27.4 – 28.2	26.5 – 27.5	25.7 – 26.8	26.4 – 27.5
MH	Sub	12.3	3.8	31.1	12.1	12.2
	σ_θ	26.5 – 27.4	27.4 – 28.2	26.5 – 27.5	25.7 – 26.8	26.4 – 27.5
LGM	Sub	16.2	8.6	43.4	10.5	24.3
	σ_θ	27.2 – 29.0	28.5 – 29.4	27.4 – 29.0	26.5 – 27.5	27.4 – 29.0